Layered Manganese Oxide Intergrowth Electrodes for Rechargeable Lithium Batteries. 1. Substitution with Co or Ni

Mickaël Dollé, Sébastien Patoux, and Marca M. Doeff*

Materials Sciences Division, Lawrence Berkeley National Laboratory, University of California, Berkeley, California 94720

Received September 9, 2004. Revised Manuscript Received November 17, 2004

Lithium manganese oxides substituted with nickel or cobalt were characterized electrochemically in lithium cell configurations. The compounds studied were either single-phase layered structures with either primarily O2 or O3 stacking arrangements, or O2/O3 intergrowths, prepared from P2, P3, and P2/P3 sodium-containing precursors, respectively. The stacking arrangements are extremely sensitive to the Na/TM (TM = transition metal) ratios and the level of substitution. Phase diagrams showing the stability regions of the various arrangements for the Na−Ni−Mn−O system are presented. A possible correlation between vacancies in the transition metal layers and electrochemical performance is suggested. For high levels of substitution with Ni, fewer defects are possible for materials containing more O3 component and higher discharge capacities can be achieved, but spinel conversion upon cycling also occurs more rapidly as the O3 content increases. Intergrowths show intermediate behavior and represent a potential route toward designing stable, high-capacity electrodes.

I. Introduction

Layered manganese oxides are of interest as positive electrode materials for lithium batteries because of their high theoretical capacities and the potential for enhanced Li ion diffusion through the two-dimensional van der Waals gaps.[1] However, orthorhombic $LiMnO_2$,[2,3] which has a corrugated structure, and monoclinic $LiMnO_2$ prepared from α-$NaMnO_2$[4,5] convert to spinel upon cycling in lithium cells. Phyllomanganates such as birnessite[6,7] or ranceite,[8] which occur naturally or may be prepared hydrothermally[9,10] or by other soft chemical techniques,[11] also undergo phase conversion.[12] The oxygen arrays in these layered structures are nearly cubic close-packed (ccp) like that of spinel, requiring only rearrangement of cations for transformation to occur. First principles calculations based on density functional theory (DFT) indicate that Mn^{2+} ions can diffuse readily through tetrahedral sites into the octahedral sites located in the lithium layers.[13] Mn^{2+} ions are produced through charge disproportionation according to eq 1.

$$2Mn^{3+}\,(\text{oct}) \rightarrow Mn^{2+}\,(\text{tet}) + Mn^{4+}\,(\text{oct}) \quad (\text{tet} = \text{tetrahedral, oct} = \text{octahedral}) \quad (1)$$

Migration requires the simultaneous presence of Mn^{3+} ions and vacancies in the lithium layers; phase conversion can be suppressed by partial substitution with ions subvalent to manganese (increasing the average oxidation state of the remaining manganese) or with multivalent ions more electronegative than Mn.[14,15] For example, $Li[Li_{0.2}Cr_{0.4}Mn_{0.4}]O_2$,[16] $Li[Ni_{0.5}Mn_{0.5}]O2$,[17] and $Li[Ni_{1/3}Mn_{1/3}Co_{1/3}]O_2$[18] all cycle stably. In each case, Mn is in the +4 oxidation state in the as-made compounds and is not redox active[19,20] under normal cycling conditions. Therefore, it may not be strictly correct to consider these materials substituted manganese oxides, but rather manganese-substituted Cr, Ni, or Ni−Co oxides.[21] More importantly, drawbacks associated with Cr (toxicity), Ni (poor abuse tolerance), and Co (cost) are still present with these materials, albeit to a lesser degree than in the unsubstituted analogues.

Another approach toward stabilization of layered manganese oxide electrodes is to employ structures that do not have

* To whom correspondence should be addressed. E-mail: mmdoeff@lbl.gov.

(1) Thackeray, M. M. *Prog. Solid State Chem.* **1997**, *25*, 1.
(2) Gummow, R. J.; Liles, D. C.; Thackeray, M. M. *Mater. Res. Bull.* **1993**, *28*, 1249.
(3) Koetschau, I.; Richard, M. N.; Dahn, J. R.; Soupart, J. B.; Rousche, J. C. *J. Electrochem. Soc.*, **1995**, *142*, 2906.
(4) Capitaine, F.; Gravereau, P.; Delmas, C. *Solid State Ionics* **1996**, *89*, 499.
(5) Armstrong, A. R.; Bruce, P. G. *Nature* **1996**, *381*, 499.
(6) Post, J. E.; Veblen, D. R. *Am. Miner.* **1990**, *75*, 477.
(7) Ohzuku, T.; Fukuda, H.; Hirai, T. *Chem. Express* **1987**, *2*, 543.
(8) Leroux, F.; Guyomard, D.; Piffard, Y. *Solid State Ionics* **1995**, *80*, 299.
(9) Chen, R.; Chirayil, T.; Zavalij, P.; Whittingham, M. S. *Solid State Ionics* **1996**, *86*−*88*, 1.
(10) Chen, R.; Zavalij, P.; Whittingham, M. S. *Chem. Mater.* **1996**, *8*, 1275.
(11) Franger, S.; Bach, S.; Pereira-Ramos, J. P.; Baffier, N. *J. Electrochem. Soc.* **2000**, *147*, 3226.
(12) Zhang, F.; Whittingham, M. S. *Electrochem. Solid State Lett.* **2000**, *3*, 309.
(13) Reed, J.; Ceder, G.; Van der Ven, A. *Electrochem. Solid State Lett.* **2001**, *4*, A78.
(14) Reed, J.; Ceder, G. *Chem. Rev.* **2004**, *104*, 4513.
(15) Reed, J. Ab Initio Study of Cathode Materials for Lithium Batteries, Ph.D. Thesis, Massachusetts Institute of Technology, 2003.
(16) Ammundsen, B.; Paulsen, J. *Adv. Mater.* **2001**, *13*, 943.
(17) Rossen, E.; Jones, C. D. W.; Dahn, J. R. *Solid State Ionics* **1992**, *57*, 311.
(18) Makimura, Y.; Ohzuku, T. *J. Power Sources* **2003**, *119*−*121*, 156.
(19) Islam, M. S.; Davies, R. A.; Gale, J. D. *Chem. Mater.* **2003**, *15*, 4280.
(20) Hwang, B. J.; Tsai, Y. W.; Carlier, D.; Ceder, G. *Chem. Mater.* **2003,** *15*, 4280.
(21) Whittingham, M. S. personal communication.

10.1021/cm048443f CCC: $30.25
Published on Web 02/08/2005

ccp arrays of oxygen. O2-Li_xMnO_{2+z} ($x \approx 0.7$, $z > 0.05$, space group $P6_3mc$), prepared from P2-$Na_{0.7}MnO_{2+z}$, has an oxygen stacking sequence of ACAB and cycles without transforming to spinel.[22,23] Recent investigations of substituted variants of this compound[24,25] indicated that some are actually intergrowths of $P6_3mc$ and $R\bar{3}m$ phases (i.e., O2 and O3) where the latter has ABC stacking (i.e., ccp oxygen arrays) like that of monoclinic $LiMnO_2$. Despite this, spinel conversion appears to be inhibited in the intergrowths, perhaps due to "pinning" by surrounding O2 layers, which may prevent the long-range ordering needed for complete transformation. Furthermore, the presence of an O3 component appears to be associated with higher capacity and/or better rate capability[26] of the electrodes. Intergrowths may represent an acceptable compromise between the phase stability of the O2 structure and the better electrochemical properties of O3, but little is currently known about them. To tailor high-capacity stable electrodes more information is needed about the conditions under which they form. To this end, we have synthesized and characterized several Ni-, Co-, or Al-substituted manganese oxides and studied their electrochemical behavior. In Part 1 we describe results with the Ni- and Co-substituted variants, and in Part 2 we describe our work on Al-substituted materials.

II. Experimental Procedures

Sodium-containing layered substituted manganese oxides, $Na_xM_yMn_{1-y}O_{2+z}$ were prepared by glycine−nitrate combustion synthesis[27] as previously described.[25,26] In brief, sodium and transition metal nitrates in the desired ratios were co-dissolved with glycine (glycine/nitrate ratio 1:2) in deionized water and heated until combustion took place. The resultant powder was heated at 800 °C for 4 h to remove any organic residue and to ensure homogeneity. For ion exchange, materials were refluxed in a solution of LiBr in ethanol (9-fold excess of Li) for 2 days. The products were washed carefully with ethanol to remove salts and dried for at least 1 day at 150°C.

Inductively coupled plasma (ICP) analyses were carried out on selected samples (Desert Analytics Laboratory, Tucson, AZ) to determine compositions. For convenience, we most commonly refer to the *nominal* compositions, unless otherwise noted.

X-ray diffraction (XRD) patterns were obtained on both the sodium-containing precursors and the ion-exchanged products using either a Siemens D5000 or a Philips X′Pert diffractometer (monochromatized Cu Kα radiation). Powdercell 2.4 by Kraus and Nolze was used to produce the theoretical patterns in the figures and unit cell parameters were determined by full pattern matching refinement using the WinPLOTR/Fullprof suite.[28] Approximate P2/P3 ratios were determined from Rietveld refinements. The considerable peak broadening observed in most of the patterns of the lithiated products precluded satisfactory refinements. Instead, an assumption was made that the O2/O3 ratios in the ion-exchanged products are similar to the P2/P3 ratios in the corresponding sodium-containing precursors. This is valid for reasons stated in the following section.

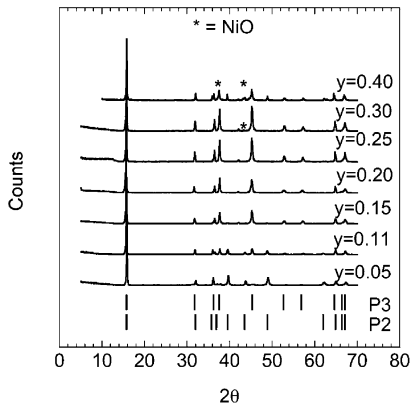

Figure 1. XRD powder patterns of $Na_{0.7}Ni_yMn_{1-y}O_{2+z}$ ($z \approx 0-0.05$) compositions, where y is varied. The expected approximate peak positions for pure P2 and P3 phases are shown as gray bars (actual positions are expected to vary somewhat with degree of Ni substitution). Peaks attributed to a NiO impurity are marked with an asterisk (*).

Positive electrodes containing 80% active material, 6% acetylene black, 6% SFG-6 graphite (Timrex Timcal), and 8% polyvinylidene fluoride (PVdF) were prepared and dried as previously described.[26] Loadings were typically 10−15 mg/cm^2 active material. Coin cells were assembled in an inert atmosphere glovebox by sandwiching together positive electrodes, Celgard 3401 separators, and lithium anodes, using 1 M $LiPF_6$ dissolved in ethylene carbonate−dimethyl carbonate (EC-DMC) as the electrolytic solution. Cells were subjected to galvanostatic cycling at 0.055 mA/cm^2 between 2.0 and 4.5 V at 21−22 °C using a MacPile II (Bio-Logic, SA, Claix, France) or an Arbin BT/HSP-2043 cycler.

III. Results and Discussion

Structural Characterization. Figure 1 shows XRD patterns of a series of Ni-substituted manganese oxides with nominal compositions, $Na_{0.7}Ni_yMn_{1-y}O_{2+z}$ ($y = 0.05-0.4$). At high Ni content ($y \geq 0.3$), NiO is present as an impurity phase but all the other patterns can be indexed to space groups $P6_3/mmc$ (P2 in layer notation) and $R3m$ (P3). Figure 2 shows the effect of varying the Na/TM ratio (where TM stands for transition metal) for two representative series, $Na_xNi_{0.11}Mn_{0.89}O_{2+z}$ (top) and $Na_xNi_{0.2}Mn_{0.8}O_{2+z}$ (bottom). Intergrowths or pure P2 and P3 phases form only within a narrow range of Na/TM ($\sim 0.7 \leq x \leq 0.8$). Outside these limits, impurity phases related to the tunnel compound, $Na_{0.44}MnO_2$, or to α-$NaMnO_2$ coexist with P2/P3 compounds, for low and high Na contents, respectively. Close to these Na/TM and Ni/(Ni + Mn) limits, nearly 100% P2 (e.g., $Na_{0.7}Ni_{0.05}Mn_{0.95}O_{2+z}$) or P3 (e.g, $Na_{0.7}Ni_{0.25}Mn_{0.75}O_{2+z}$) phases are formed, with only traces of the secondary component. In general, higher P3 contents are found when either the Ni content is raised or the Na content is lowered and vice versa. An apparent exception is seen in the $y = 0.4$ phase mixture. However, the true composition of the layered component in that sample is actually $Na_{(0.7/(1-w))}Ni_{((0.4-w)/(1-w))}Mn_{(0.6/(1-w))}O_2$, where w represents the mole fraction of NiO impurity (close to 0.1). The increase in P2 content is consistent with the higher-than-expected Na content and lower-than-expected Ni content for the layered component of this mixture.

(22) Paulsen, J. M.; Thomas, C. L.; Dahn, J. R. *J. Electrochem. Soc.* **1999**, *146*, 3560.
(23) Shaju, K. M.; Subba Rao, G. V.; Chowdari, B. V. R. *Electrochem. Commun.* **2002**, *4*, 633.
(24) Eriksson, T. A.; Doeff, M. M. *J. Power Sources* **2003**, *119−121*, 145.
(25) Eriksson, T. A.; Lee, Y. J.; Hollingsworth, J.; Reimer, J. A.; Cairns, E. J.; Zhang, X.-F.; Doeff, M. M. *Chem. Mater.* **2003**, *15*, 4456.
(26) Dollé, M.; Hollingsworth, J.; Richardson, T. J.; Doeff, M. M. *Solid State Ionics* **2004**, *175/1-9*, 225.
(27) Chick, L. A.; Pederson, L. R.; Maupin, G. D.; Bates, J. L.; Thomas, L. E.; Exarhos, G. J. *Mater. Lett.* **1990**, *10*, 6.
(28) WinPLOTR software. http://www-llb.cea.fr/fullweb/winplotr/winplotr.htm.

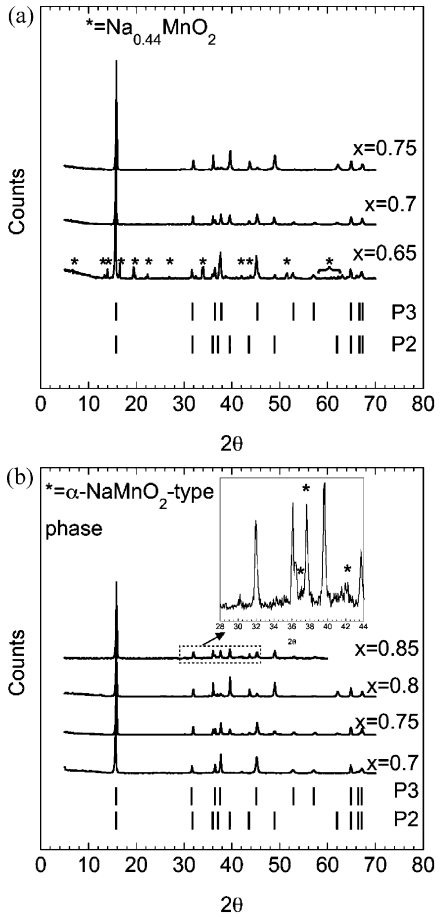

Figure 2. XRD powder patterns of (a) $Na_xNi_{0.11}Mn_{0.89}O_{2+z}$ and (b) $Na_xNi_{0.2}Mn_{0.8}O_{2+z}$ compositions, where *x* is varied. The expected approximate peak positions for pure P2 and P3 phases are shown as gray bars (actual positions are expected to vary somewhat with Na content). Peaks attributed to $Na_{0.44}MnO_2$ or α-$NaMnO_2$ impurities are marked with an asterisk (*).

Figure 3 shows the approximate *nominal* composition ranges for layered P2/P3 intergrowths in the Na−Ni−Mn−O system. In practice, actual compositions (in particular, sodium contents) differ somewhat from the nominal ones, as shown in Table 1 for several samples analyzed by ICP. Sodium is lost during combustion and calcination at elevated temperatures.

Similar trends are seen for $Na_xCo_yMn_{1-y}O_{2+z}$ compounds, although the composition ranges are somewhat different than those found for $Na_xNi_yMn_{1-y}O_{2+z}$ (Figure 4).

Table 2 lists fractions of P2 components and P2 and P3 lattice parameters determined for $Na_xM_yMn_{1-y}O_{2+z}$ compositions that do not contain other phases. These values are valid for single-phase materials and compounds that are primarily "zone" intergrowths in which a fairly large P3 moiety is sandwiched between P2 components in individual grains, as is shown in Figure 5 of ref 25. More sophisticated refinement techniques than were used here, however, are required to determine the true compositions of materials containing a large fraction of grains in which the two phases are more intimately mixed. Due to the structural similarity of P2 and P3 arrangements, the latter are difficult to detect even by TEM, although the analysis described in ref 25 indicates that a plurality of grains in the samples examined are of the zone intergrowth type. Due to this caveat, the values listed in Table 2 should be considered estimates of the true phase compositions of the intergrowth materials.

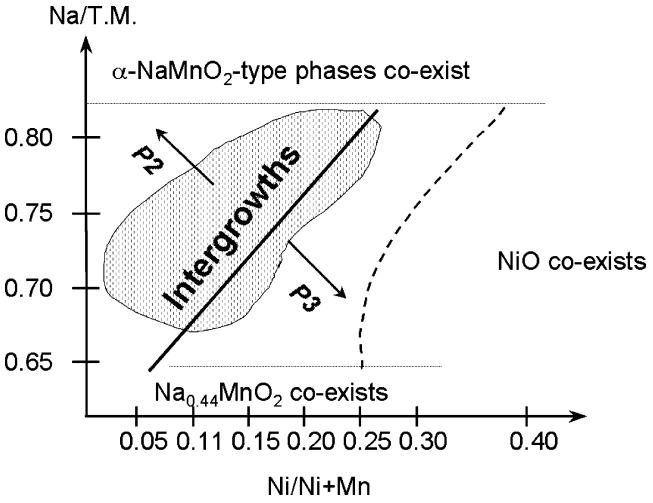

Figure 3. Diagram showing approximate nominal composition range of layered P2/P3 intergrowths in the Na−Ni−Mn−O system.

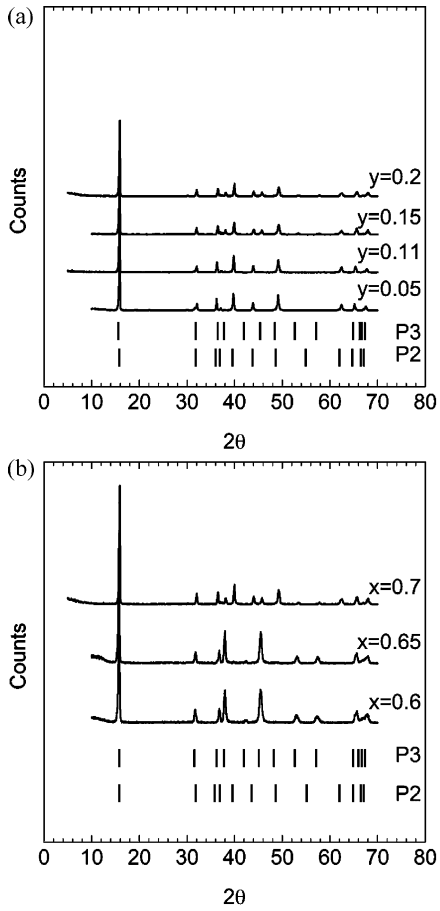

Figure 4. (a) XRD powder patterns of $Na_{0.7}Co_yMn_{1-y}O_{2+z}$ ($z \approx 0-0.05$) compounds, where *y* is varied, and (b) $Na_xCo_{0.2}Mn_{0.8}O_{2+z}$ compounds where *x* is varied. The expected approximate peak positions for pure P2 and P3 phases are shown as gray bars (actual positions are expected to vary somewhat with degree of Co substitution and Na content).

Partial replacement of Mn with subvalent ions should reduce the overall unit cell volumes in proportion to the degree of substitution (Vegard's law)[29] because larger Mn^{3+} ions are replaced by smaller Mn^{4+} ones ($r(Mn^{3+}) = 0.645$ Å, $r(Mn^{4+}) = 0.53$ Å)[30] provided that the substituting ions

(29) Jenkins, R.; Snyder, R. L. *Introduction to X-ray Powder Diffractometry*; John Wiley & Sons: New York, 1996; p 42.
(30) Shannon, R. D.; Prewitt, C. T. *Acta Crystallogr.* **1969**, *B25*, 925.

Table 1. Nominal and Actual Compositions of Selected Ni-Substituted Phases

	compositions determined by ICP	
nominal composition	before ion-exchange	after ion-exchange
$Na_{0.7}Ni_{0.2}Mn_{0.8}O_2$	$Na_{0.49}Ni_{0.18}Mn_{0.82}O_{2+z}$	$Li_{0.64}Na_{0.01}Ni_{0.18}Mn_{0.82}O_{2+z}$
$Na_{0.75}Ni_{0.2}Mn_{0.8}O_2$	$Na_{0.59}Ni_{0.19}Mn_{0.81}O_{2+z}$	$Li_{0.65}Na_{0.02}Ni_{0.19}Mn_{0.81}O_{2+z}$
$Na_{0.8}Ni_{0.2}Mn_{0.8}O_2$	$Na_{0.62}Ni_{0.19}Mn_{0.81}O_{2+z}$	$Li_{0.73}Na_{0.05}Ni_{0.19}Mn_{0.81}O_{2+z}$

Table 2. Unit Cell Parameters of $Na_xM_yMn_{1-y}O_{2+z}$ (M = Ni, Co): Space Groups $P6_3/mmc$ (P2) and $R3m$ (P3)

		P2 lattice parameters[a]		P3 lattice parameters	
nominal composition	% P2	*a* (Å)	*c* (Å)	*a* (Å)	*c* (Å)
$Na_{0.7}Ni_{0.05}Mn_{0.95}O_2$	>95	2.872(1)	11.192(26)	2.862(4)[a]	16.796(15)[a]
$Na_{0.7}Ni_{0.11}Mn_{0.89}O_2$	~65	2.871(1)	11.209(15)	2.867(2)	16.831(16)
$Na_{0.75}Ni_{0.11}Mn_{0.89}O_2$	~90	2.871(1)	11.194(7)	2.874(6)	16.752(19)
$Na_{0.7}Ni_{0.15}Mn_{0.85}O_2$	~35	2.872(1)	11.219(15)	2.868(1)	16.881(14)
$Na_{0.7}Ni_{0.2}Mn_{0.8}O_2$	<5	2.874(1)[a]	11.308(30)[a]	2.873(3)	16.943(18)
$Na_{0.75}Ni_{0.2}Mn_{0.8}O_2$	52	2.875(1)	11.223(10)	2.877(1)	16.785(10)
$Na_{0.8}Ni_{0.2}Mn_{0.8}O_2$	84	2.871(1)	11.196(6)	2.880(6)	16.768(30)
$Na_{0.7}Ni_{0.25}Mn_{0.75}O_2$	<5	2.875(1)[a]	11.239(21)[a]	2.874(2)	16.864(10)
$Na_{0.7}Co_{0.05}Mn_{0.95}O_2$	>95	2.860(1)	11.146(8)	2.848(10)[a]	16.914(24)[a]
$Na_{0.7}Co_{0.11}Mn_{0.89}O_2$[b]	~94	2.8524(3)	11.161(3)	2.85[a]	16.72[a]
$Na_{0.7}Co_{0.15}Mn_{0.85}O_2$	~82	2.845(1)	11.185(11)	2.838(2)	16.781(15)
$Na_{0.6}Co_{0.2}Mn_{0.8}O_2$	trace	2.847(2)[a]	11.256(42)[a]	2.846(3)	16.912(24)
$Na_{0.65}Co_{0.2}Mn_{0.8}O_2$	<5	2.847(2)[a]	11.274(36)[a]	2.848(3)	16.877(21)
$Na_{0.7}Co_{0.2}Mn_{0.8}O_2$	~80	2.845(1)	11.188(11)	2.837(2)	16.787(16)

[a] Estimated values (e.g., for minority (<5%) phases). [b] From ref 25.

are similar in size to Mn^{3+}. Cell volumes shrink with a greater degree of substitution in $Na_xCo_yMn_{1-y}O_{2+z}$ suggesting that the Co^{3+} ion, rather than the larger Co^{2+} ($r(Co^{3+}) = 0.61$ Å, $r(Co^{2+}) = 0.745$ Å), is present (Figure 5a). In contrast, the unit cell volumes expand up to about $y = 0.2$ when M = Ni, after which point they become smaller. Thus, it is likely that Ni substitutes as the larger +2 ion, rather than as +3 ($r(Ni^{2+}) = 0.69$ Å, $r(Ni^{3+}) = 0.60$ Å), which partially counteracts the effect of increasing amounts of Mn^{4+} until substitution levels are high. This also provides an explanation for the rather low *y* composition limit in the $Na_{0.7}Ni_yMn_{1-y}O_{2+z}$ series because high values would require an unlikely average oxidation state above +4 for Mn. These examples are similar to the situation with $LiNi_{1/3}Co_{1/3}Mn_{1/3}O_2$, in which the predominant oxidation states have been determined by X-ray photoelectron spectroscopy to be +2 for Ni and +3 for Co.[31] It is interesting to note that roughly similar trends are observed for both the P2 and P3 components, although there is some scatter in the data. This suggests that the substituents are distributed fairly evenly between the two stacking arrangements rather than being segregated into two components as in the composite materials, $xLi_2MnO_3 \cdot (1-x)LiMn_{0.5}Ni_{0.5}O_2$.[32]

Varying the Na content has only a minor impact on the unit cell volumes for the three series $Na_xNi_{0.11}Mn_{0.89}O_{2+z}$, $Na_xNi_{0.2}Mn_{0.8}O_{2+z}$, and $Na_xCo_{0.2}Mn_{0.8}O_{2+z}$ shown in Figure 5b. Instead, this affects the relative amounts of P2 and P3 in the intergrowths (Table 2), suggesting that the sodium contents of each are somewhat different and are fixed for each phase within a very narrow range.

The existence of P2/P3 intergrowths for several quaternary Na−M−Mn−O systems within certain composition ranges suggests similar energetics for formation of these two different stacking arrangements. In the Na−Mn−O system, the hexagonal P2 phase commonly forms when vacancies are present in both the sodium and transition metal layers; *z* in unsubstituted P2−$Na_{0.7}MnO_{2+z}$ is normally between 0.05 and 0.25 for materials prepared below 600 °C.[33] This has the effect of raising the average Mn oxidation state, thus minimizing the number of Jahn−Teller Mn^{3+} ions. Above 600 °C, β-$Na_{0.7}MnO_{2+z}$ ($z \leq 0.05$) with an orthorhombically or monoclinically[34] distorted structure forms, and can be designated P′2. This phase is stable only at elevated temperatures and reversibly oxidizes to form the P2 phase during slow cooling in air.[34]

The number of cationic deficiencies in the TM layers is dependent upon the temperature and oxygen partial pressure used during synthesis, and *x* in Na_xMnO_{2+z} is fixed near 0.7, but the exact value can also vary depending upon the synthetic conditions. (For example, elemental analysis and density measurements give $Na_{0.63}MnO_{2.02}$ as the composition for a 100% P2 material made under the same conditions as those in this study).[35] P2-$Na_{0.7}MnO_{2+z}$ may be written more accurately as $Na_{0.7((2/(2+z))}Mn_{(2/(2+z)}O_2$, indicating the presence of vacancies, rather than implying an oxygen excess.[36] Figure 6a shows the effect of varying *z* on the average Mn oxidation state for the idealized P′2 or P2 compound, $Na_{0.7}MnO_{2+z}$ or $Na_{0.7((2/(2+z))}Mn_{(2/(2+z)}O_2$, (heavy dark line).

Substitution with ions subvalent to Mn increases the average oxidation state. Assuming an oxidation state of +2 for Ni, composition lines for $Na_{0.7}Ni_yMn_{1-y}O_{2+z}$, (shown for $y = 0.1$, 0.2, and 0.3 as light black lines) can be drawn running roughly parallel to the one for P2-$Na_{0.7}MnO_{2+z}$ but shifted upward. Above about $y = 0.07$, the compositional

(31) Shaju, K. M.; Subba Rao, G. V.; Chowdari, B. V. R. *Electrochim. Acta* **2002**, *48*, 145.
(32) Kim, J.-S.; Johnson, C. S.; Vaughey, J. T.; Thackeray, M. M. *Chem. Mater.* **2004**, *16*, 1996.
(33) Parant, J.-P.; Olazcuaga, R.; Devalette, M.; Fouassier, C.; Hagenmuller, P. *J. Sol. State. Chem.* **1971**, *3*, 1.
(34) Paulsen, J. M.; Dahn, J. R. *Solid State Ionics* **1999**, *126*, 3.
(35) Patoux, S.; Dollé, M.; Doeff, M. M. *Chem. Mater.* **2005**, *17*, 1044.
(36) Mendiboure, A.; Delmas, C.; Hagenmuller, P. *J. Solid State Chem.* **1985**, *57*, 323.

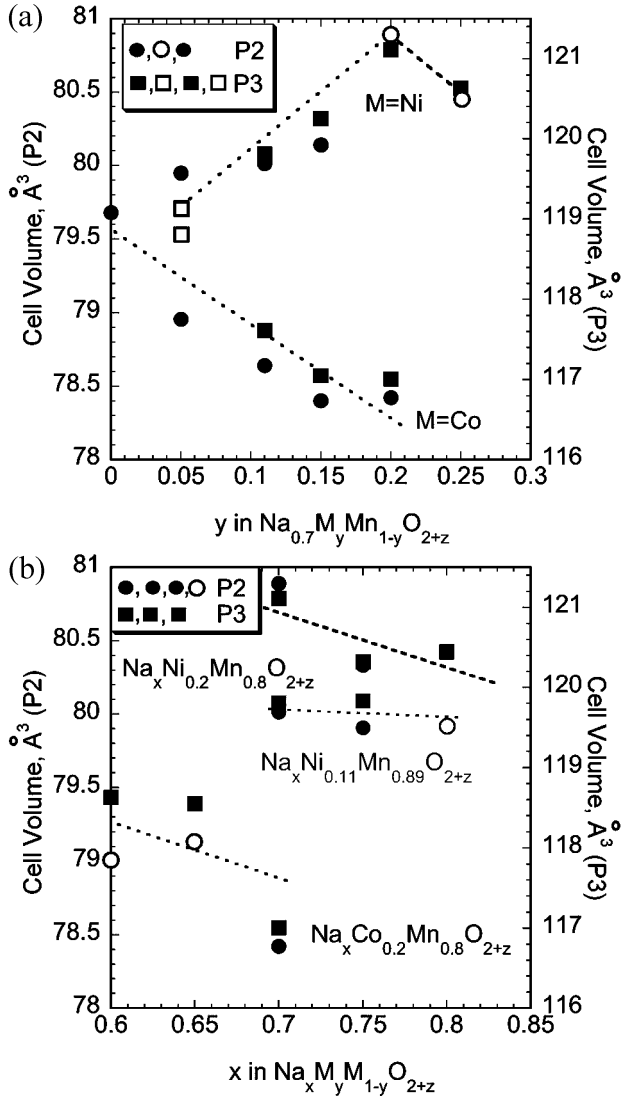

Figure 5. (a) P2 and P3 unit cell volumes as a function of Ni or Co content in $Na_{0.7}M_yMn_{1-y}O_{2+z}$ (M = Ni, Co) compounds: P2 values are shown as circles (estimated values as open circles) and P3 values are shown as squares (estimated values as open squares). Data for Ni substitution are shown in black and those for Co substitution are in gray. Dashed lines are meant as a guide to the eye only. Data for P2-$Na_{0.7}MnO_{2+y}$ are taken from ref 25. (b) P2 and P3 unit cell volumes as a function of Na content in $Na_xNi_{0.2}Mn_{0.8}O_{2+z}$ (black), $Na_xNi_{0.11}Mn_{0.89}O_{2+z}$ (light gray), and $Na_xCo_{0.2}Mn_{0.8}O_{2+z}$ (dark gray) compounds. Symbols are the same as in (a) and dashed lines are provided as a guide to the eye.

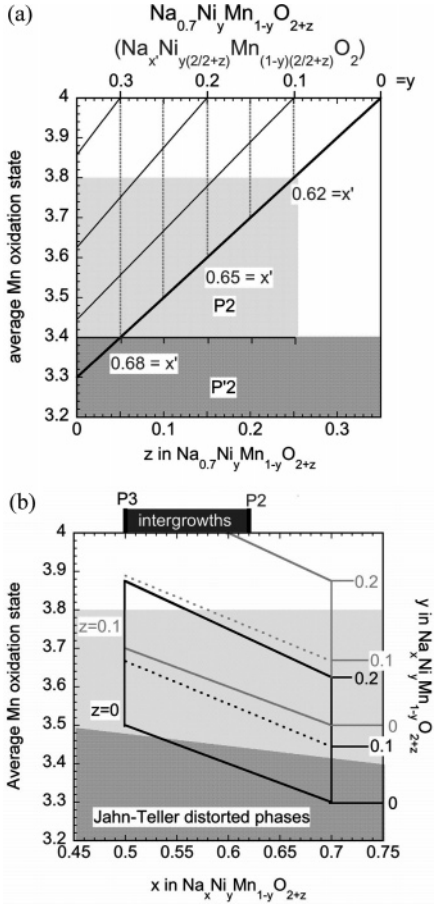

Figure 6. (a) Average Mn oxidation state as a function of z (see text) of the defect line phase P2-$Na_{0.7}MnO_{2+z}$ and hypothetical P2 phases, $Na_{0.7}Ni_yMn_{1-y}O_{2+z}$ (—). Tie lines representing constant values of x' (- - - -) in $Na_{x'}Ni_{y(2/2+z)}Mn_{(1-y)(2/2+z)}O_2$ (crystallographic formula) are included. Compositions on lines falling within the dark gray shaded region are expected to have distorted P′2 structures and those in the light gray shaded area are expected to have P2 structures. (b) Average Mn oxidation state as a function of x, y, and z for the $Na_xNi_yMn_{1-y}O_{2+z}$ system.

lines fall outside the expected region for P′2, where the average Mn oxidation state is below 3.4, shown as a dark gray area in the graph. This is in accord with experimental evidence showing that P′2 phases do not form for $Na_{0.7}Ni_yMn_{1-y}O_{2+z}$ compounds with high y.[34]

Compositions that fall on these parallels are expected to form pure P2 structures, particularly in the light gray shaded area in Figure 6a indicating easily obtainable Mn oxidation states and numbers of vacancies. For high levels of substitution, lines may fall completely above the shaded region implying that P2 phases without such defects can form (e.g., $Na_{2/3}Ni_{1/3}Mn_{2/3}O_2$ in ref 37).

When the actual Na/TM ratio is not 0.7 (for the idealized case), P3 structures, P2/P3 intergrowths, or phase mixtures occur. Pure P3 structures also appear to behave as line phases and exist when the true Na/TM ratio is close to 0.5 (with the exact value again depending upon details of the synthesis and substitution),[35,38] while intergrowths form in the approximate range $0.5 < \text{Na/TM} < 0.7$. A graph similar to the one in 6a can be constructed for $Na_{0.5}Ni_yMn_{1-y}O_{2+z}$ and shows that lines for lower substitution levels (e.g., $y \approx 0.2$) fall within the "low vacancy" zone above the shaded area. Figure 6b summarizes the effect of changing x, y, and z in the $Na_xNi_yMn_{1-y}O_{2+z}$ system upon the Mn oxidation state and shows that $z \approx 0$ for P3 phases at high Ni substitution levels, but can be nonzero for P2 or intergrowths, because x is increased. The situation is less clear-cut for lower values of y or substitution with +3 ions such as Co or Al,[35] where it is theoretically possible for P3 phases to have vacancies as well.

Upon exchange of Na for Li, P2 and P3 stacking arrangements convert to O2 and O3, respectively. Transition metal layers need only to glide to change the alkali metal environment from prismatic to octahedral coordination, which better accommodates the smaller Li^+ ion. Conversion

(37) Paulsen, J. M.; Dahn, J. R. *J. Electrochem. Soc.* **2000**, *146*, 3560.

(38) Robertson, A. D.; Armstrong, A. R.; Bruce, P. G. *Chem. Mater.* **2001**, *13*, 2380.

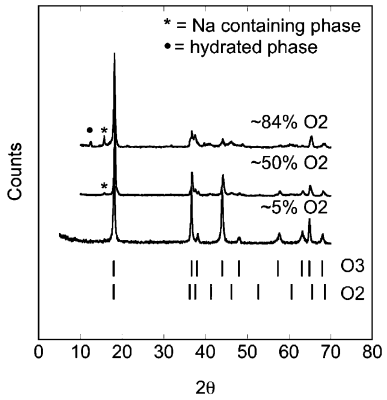

Figure 7. XRD powder patterns of ion-exchanged compounds made from $Na_{0.8}Ni_{0.2}Mn_{0.8}O_2$ (top), $Na_{0.75}Ni_{0.2}Mn_{0.8}O_2$ (middle), and $Na_{0.7}Ni_{0.2}Mn_{0.8}O_2$ (bottom). (See Table 1 for actual compositions). The expected approximate peak positions for pure O2 and O3 phases are shown as gray bars. A Na-containing phase is marked with an asterisk (*) and a hydrated phase is marked with a dot (●).

of P2 to O3, or P3 to O2, requires substantial rearrangement of the lattice and will not occur under the mild conditions used for exchange in this study. Thus, we can assume that the O2/O3 ratios in the ion-exchanged products remain the same as the P2/P3 ratios in the corresponding sodium-containing precursors.

Figure 7 shows XRD powder patterns of ion-exchanged materials made from the series with nominal compositions of $Na_xNi_{0.2}Mn_{0.8}O_2$, and Table 1 lists their true compositions determined by ICP. As the O2/O3 ratio increases, more residual sodium is found in the products and weak reflections attributable to a second layered phase with larger unit cell parameters are observed in the XRD patterns. This is most likely a phase containing primarily sodium, although it is also possible for sodium ions to be present in lithiated phases and vice versa. These ions are likely to be segregated into different layers because of size differences, causing O2/P2 stacking faults. Both O2/P2 and O2/O3 faults result in line broadening, readily observable particularly in the top pattern in Figure 7. Note that line broadening is also seen in patterns of the P2/P3 intergrowths (Figures 1, 2, and 4).

Electrochemical Characterization. Lithium cells containing the layered ion-exchanged materials typically have open circuit potentials of about 3.3 V, and may either be partially discharged or charged initially. Figure 8 shows a partial charge and subsequent discharge at low current densities of three lithium cells containing the exchanged products of the compounds with nominal compositions of $Na_xNi_{0.2}Mn_{0.8}O_2$, whose XRD powder patterns are shown in Figure 7 and whose true compositions are listed in Table 1. Less lithium can be extracted upon charge for the compound that is mostly O2, reducing the available capacity during the following discharge. The impedance also appears to be greater for this cell, judging from the separation between charge and discharge traces, which suggests there are transport limitations associated with the large O2 component in this cathode material. The inability to exchange this compound completely and to charge it fully in cells indicates that some of the alkali metal ions in the van der Waals gaps are immobile. The immobility is due to the presence of vacancies, which act as

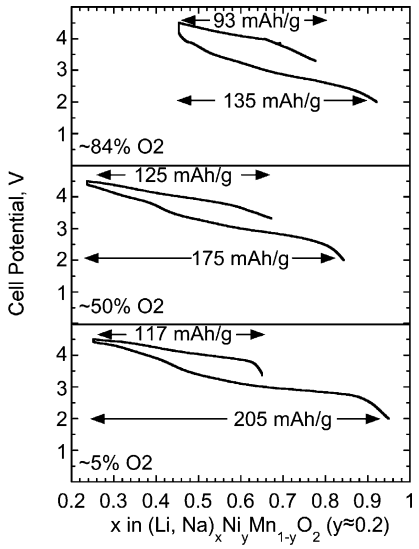

Figure 8. Initial charges and subsequent discharges, at 0.055 mA/cm^2, of lithium cells containing ion-exchanged compounds made from $Na_{0.8}Ni_{0.2}Mn_{0.8}O_2$ (top), $Na_{0.75}Ni_{0.2}Mn_{0.8}O_2$ (middle), and $Na_{0.7}Ni_{0.2}Mn_{0.8}O_2$ (bottom). (See Table 1 for actual compositions).

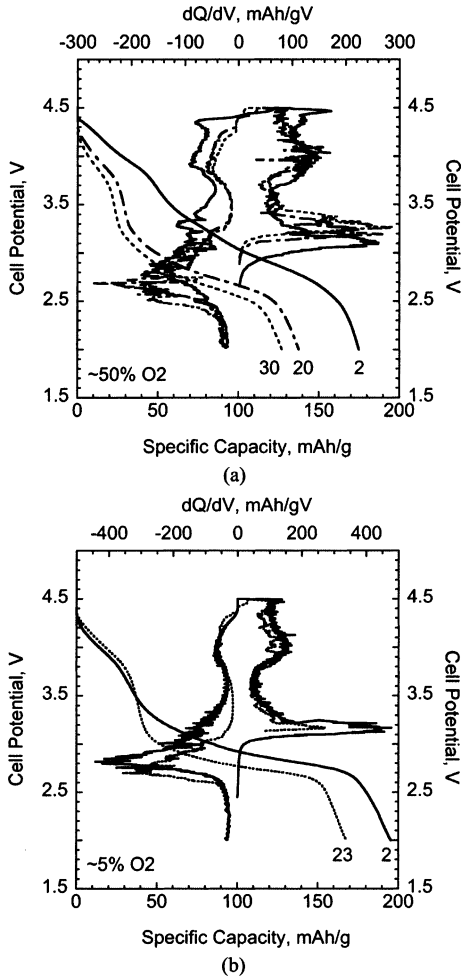

Figure 9. Discharges at 0.055 mA/cm^2 of lithium cells containing (a) $Li_{0.65}Na_{0.02}Ni_{0.19}Mn_{0.81}O_{2+z}$ made from $Na_{0.59}Ni_{0.19}Mn_{0.81}O_{2+z}$ and (b) $Li_{0.64}Na_{0.01}Ni_{0.18}Mn_{0.82}O_{2+z}$ made from $Na_{0.49}Ni_{0.18}Mn_{0.82}O_{2+z}$ (actual compositions). Cycle numbers are labeled. Incremental capacity plots for the corresponding full cycles are superimposed.

effective negative charges in the transition metal layers and trap ions.[38] Because the number of vacancies for the O3 components of compounds in this series is very low, ion

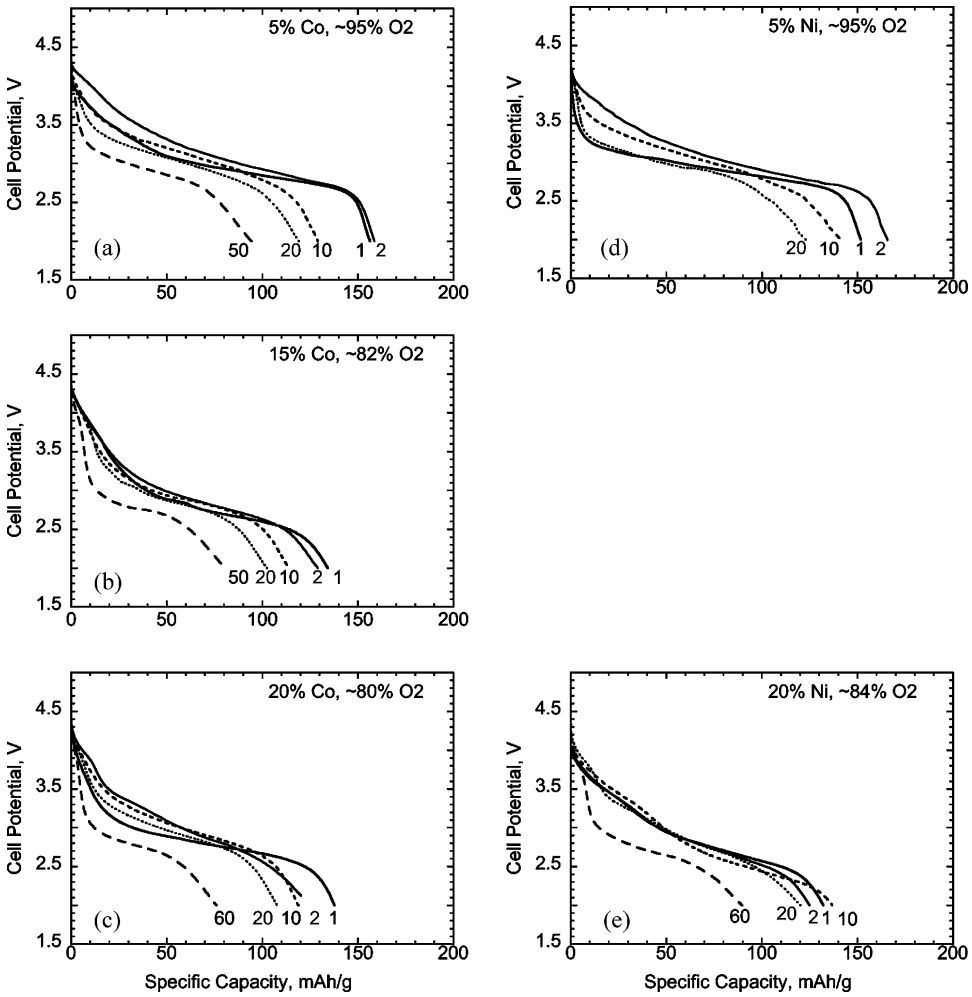

Figure 10. Discharges at 0.055 mA/cm^2 of lithium cells containing substituted O2/03 compounds: (a) $Li_xCo_{0.05}Mn_{0.95}O_2$, ~95% O2; (b) $Li_xCo_{0.15}Mn_{0.85}O_2$, ~82% O2; (c) $Li_xCo_{0.2}Mn_{0.8}O_2$, ~80% O2; (d) $Li_xNi_{0.05}Mn_{0.95}O_2$, ~95% O2; and (e) $Li_{0.73}Na_{0.05}Ni_{0.19}Mn_{0.81}O_{2+z}$ made from $Na_{0.62}Ni_{0.19}Mn_{0.81}O_{2+z}$ (actual composition), ~84% O2. Cycle numbers are marked.

exchange is more complete and more capacity is obtained during electrochemical cycling.

Nearly all of the lithium can be extracted from the compound containing the most O3 component (Figure 8, bottom). When x is approximately 0.35 in $Li_xNi_{0.2}Mn_{0.8}O_2$, all of the Mn is in the +4 state, so that oxidation past this point requires participation of Ni. The high discharge capacity (>200 mAh/g) is only possible, however, if Mn is also electroactive. Thus, although $LiNi_{0.5}Mn_{0.5}O_2$ has the same structure as O3-$Li_xNi_{0.2}Mn_{0.8}O_2$, the electrochemistry is quite different, because only Ni is redox active in the first compound.

Materials with O3 stacking arrangements can be expected to undergo conversion to the spinel phase upon cycling. Armstrong et al.[39] have shown that partial substitution does not prevent this phase-transition in compounds structurally related to the ones in this study, although it may delay it. Spinel formation also occurs in intergrowths with a large fraction of O3 component, although the rate progressively slows as the O2 content increases. A two-plateau potential profile, characteristic of spinel, develops after about 20 cycles for the material containing about 5% O2 (Figure 9, bottom) but still has not evolved completely after 30 cycles for the one containing 52% O2 (Figure 9, top). Capacity near 4 V is evident on the first cycle, particularly in the differential capacity plots, but is attributable to redox processes of Ni, rather than phase transformation, as the voltage profile is still sloping. Sharpening of the peaks below 3 V in the dQ/dV data (particularly evident in the plot at the bottom of Figure 9) is an indication of conversion and corresponds to the development of the two spinel plateaus.

Because of this strong tendency to undergo phase transformation, compounds with high O3 content (corresponding to low P2 content materials listed in Table 2) were omitted from further study. The electrochemistry of compounds substituted with 11% Co or Ni has also been described in ref 25 and is not repeated here. Discharge profiles of the remaining exchanged compounds are presented in Figure 10. These compounds are all primarily O2 and do not undergo spinel conversion upon cycling. (Compare, for example, Figure 9 with Figure 10e, for the entire 20% Ni-substituted series with varying O2 content). Capacities are significantly lower than theoretical, however, and fading occurs rapidly upon cycling, as is typical for many compounds with primarily O2 stacking arrangements. Optimization of the relative amounts and the arrangements of O2 and O3

(39) Armstrong, R. A.; Robertson, A. D.; Gitzendanner, R.; Bruce, P. G. *J. Solid State Chem.* **1999**, *145*, 549.

components in intergrowths will be necessary to design stable, high-capacity, layered manganese oxide cathodes. Additionally, some consideration needs to be given to the effect of substitution and synthetic conditions on the numbers of vacancies and their role in determining the electrochemical characteristics. It is interesting to note that compounds derived from P2-$Na_{2/3}Ni_{1/3}Mn_{2/3}O_2$, which is vacancy-free, perform well electrochemically.[37]

While partial replacement of Mn with Ni or Co allows formation of intergrowths, poor abuse tolerance, in the case of Ni, and cost considerations, in the case of Co, make materials containing these metals undesirable for electric or hybrid vehicle applications. Reference 25 indicates that intergrowths also form when Al, Li, or Fe are used as substituents. Complete removal of lithium from layered manganese oxide structures containing some Al is unlikely to occur, preventing irreversible and potentially dangerous side-reactions associated with high states-of-charge, such as electrolyte oxidation or loss of oxygen from the cathode. The potential for improved abuse-tolerance as well as low cost and low toxicity makes Al-substituted manganese oxides an attractive option for a systematic analysis of intergrowth electrodes. In part 2 of this study, we describe recent work on single phase and intergrowth electrodes in the $Li_xAl_yMn_{1-y}O_{2+z}$ system.

IV. Conclusions

Layered lithium-containing substituted manganese oxides can be prepared from sodium-containing precursors, $Na_xM_yMn_{1-y}O_{2+z}$ (M = Ni, Co). XRD data suggest that Ni substitutes in the +2 oxidation state, while Co is present as the +3 ion. The stacking arrangements obtained are very sensitive to the values of x and y in the above formula. P2 and P3 structures appear to be line phases, which form when x is close to 0.7 and 0.5, respectively, whereas P2/P3 intergrowths form at intermediate values of x. Ion-exchange causes sliding of the transition metal layers, converting P2 to O2 and P3 to O3 stacking arrangements. Initial discharge capacities over 200 mAh/g are obtained for cells containing a 20% Ni substituted cathode with a primarily O3 structure, but conversion to spinel is rapid. Capacities decrease for intergrowths containing more O2 component, but spinel conversion is slower or does not occur. A possible role for vacancies in determining the electrochemical behavior is suggested.

Acknowledgment. This work was supported by the Assistant Secretary for Energy Efficiency and Renewable Energy, Office of FreedomCAR and Vehicle Technologies of the U.S. Department of Energy under Contract DE-AC03-76SF00098.

CM048443F